# Construction of cosmic string induced temperature anisotropy maps with CMBFAST and statistical analysis

N. Simatos*
*Department of Physics, University of Crete, GR–71003 Heraklion, Crete, Greece*

L. Perivolaropoulos†
*Institute of Nuclear Physics, National Centre for Scientific Research, Demokritos N.C.S.R., Athens, Greece*

(Received 21 December 1999; published 27 December 2000)

We use the publicly available code CMBFAST, as modified by Pogosian and Vachaspati, to simulate the effects of wiggly cosmic strings on the cosmic microwave background (CMB). Using the modified CMBFAST code, which takes into account vector modes and models wiggly cosmic strings by the one-scale model, we go beyond the angular power spectrum to construct CMB temperature maps with a resolution of a few degrees. The statistics of these maps are then studied using conventional and recently proposed statistical tests optimized for the detection of hidden temperature discontinuities induced by the Gott-Kaiser-Stebbins effect. We show, however, that these realistic maps cannot be distinguished in a statistically significant way from purely Gaussian maps with an identical power spectrum.

DOI: 10.1103/PhysRevD.63.025018 PACS number(s): 11.27.+d, 98.80.Cq

## I. INTRODUCTION

A promising method of identifying the origin of the large-scale structure of the universe is the statistical analysis of the cosmic microwave background (CMB) fluctuations [1–5]. What one hopes to get out of this is the possible distinction between the two major classes of physical theories of structure formation, namely, theories of inflation [6] and topological defects [7]. An important differentiating feature of these two classes of theories is the statistics of primordial fluctuations. Temperature anisotropies $\Delta T/T$ of the CMB, if originating from quantum fluctuations in an inflationary context, should obey Gaussian statistics. However, the confidence by which the CMB anisotropies were shown to follow that statistic is reduced [8], keeping in mind the work done by [9,10] using cosmic background explorer (COBE) differential microwave radiometer (DMR) maps. This could favor topological defect theories.

Cosmic strings seeding structure formation [11–15] make a promising case for these theories. However, despite the significant progress made recently [12,13,16–18] in understanding the effects of cosmic strings on the CMB, the uncertainty of the derived predictions remains significant [19,20]. The main source of this uncertainty is that there is no simple way to characterize the network of strings. In order to bypass this difficulty, various studies have attempted to model the string network by incorporating simplifying assumptions. Such simplifications have made possible the realization of cosmological string network simulations [21–23] that attempt to model evolution in a very wide range of scales. They have also made possible the construction of semianalytical models that attempt to capture features missed by the inherent limitations of full scale numerical simulations. For example, early work [24,25] based on the latter approach had revealed important features of the cosmic string induced CMB fluctuations that were missed by detailed numerical simulations. In particular it was shown [25] that, using a simple model of string network evolution, the wiggles (small scale structure) of long cosmic strings tend to amplify the height of the Doppler peak of the CMB angular spectrum of string induced fluctuations.

The main reason for this amplification may be attributed to the two main factors that determine the string induced fluctuations. These are, first the integrated Sachs–Wolfe effect (long strings present between the last scattering and the present time, gravitationally interacting directly with the photons), for scales larger than 2 degrees, and second, for scales of about 1–2 degrees, interactions of the photons with string perturbed plasma performing acoustic oscillations on the last scattering surface (LSS) excited by long strings. It may be shown [25–27] that the latter effect leads to temperature fluctuations $\Delta T/T$ that are amplified compared to the fluctuations induced by the former effect. The amplification factor $\lambda > 1$ is due to the fact that the wiggles do not gravitationally interact directly with the photons, while they do interact with the plasma [25,27] on the LSS, leading indirectly to additional fluctuations on the CMB through the last scattering of photons on the fast moving plasma electrons. Therefore, this amplification can only affect the last scattering horizon scale, i.e., a scale of about 1–2 degrees. The factor $\lambda$ can be expressed as [25,27]

$$\lambda = \left( 1 + \frac{\left(1 - \frac{T}{\mu}\right)}{2\langle (v_s \gamma_s)^2 \rangle} \right), \tag{1.1}$$

where $T$ is the tension of the wiggly long string which decreases with the wiggliness and is estimated by simulations to be $T \simeq 0.7\mu$ where $\mu$ is the mass per unit length of the string. Also, $v_s$ is the string velocity and $\gamma_s$ the corresponding Lorentz factor.

*Email address: simatos@physics.uoc.gr
†Email address: leandros@mail.demokritos.gr

 

This result of Doppler peak amplification due to cosmic string wiggles has recently been verified by the numerical modeling developed by Pogosian and Vachaspati [26]. These authors used the line of sight integration approach of the publicly available code CMBFAST [28], combined with the one-scale model [29,30] for wiggly cosmic string evolution, to derive the angular CMB power spectrum and the matter power spectrum. One of their main results was that small scale structure (wiggles) of long strings tend to increase the height of the Doppler peak of the CMB spectrum, thus confirming the expectations of Ref. [25] and improving the agreement of the predicted angular spectrum with observations.

In the present work we use the approach of Pogosian and Vachaspati, and modify their publicly available code based on CMBFAST to go beyond the CMB spectrum and construct realistic maps of CMB fluctuations produced by wiggly strings. Our goal is to apply statistical tests on several realizations of these maps and attempt to identify their non-Gaussian features. Some of the tests we applied [31] (which were specially designed for this purpose) were able to identify non-Gaussian features on simple CMB maps [9], constructed by the superposition of a small temperature discontinuity (produced by a single long string via the Gott-Kaiser-Stebbins effect [32,33]) on a Gaussian background. In the present study, however, we show that these same tests are not able to identify the string induced non-Gaussianity of more realistic maps on the scales considered. This is due to the fact that the superposition of several line-like temperature discontinuities tends to wash out the effects of each individual discontinuity and reduces the effectiveness of the proposed tests. Therefore, the detection of the small non-Gaussianity induced by cosmic strings on a few degrees scale remains a challenging open issue.

## II. CONSTRUCTION OF THE MAPS

The construction of the CMB temperature anisotropy maps, on which the statistical tests were performed, was made possible by two major contributions: the wiggly string one-scale model as the cosmic string network model and the use of the line of sight integration approach.

The cosmic string network model that we used is the one found in detail in [26]. Briefly, the network is approximated [12–14] by a collection of uncorrelated straight string segments which are assumed to be produced at some early epoch, with positions drawn randomly from a uniform distribution in space, moving with random uncorrelated velocities, their directions drawn from a uniform distribution on a two sphere. This model has the merit of being relatively simple and amenable to modifications that seem to be indicated by direct simulations [23,34].

Small-scale structures, wiggles, were incorporated in order to make the model more realistic, since lattice simulations of string formation and evolution [23] suggest that strings are not straight. However, a distant observer would not be able to discern this small-scale structure, seeing instead a smooth string with effective mass per unit length $\tilde{U}$ and tension $\tilde{T}$. The wiggly string is heavier and slower than the ordinary Nambu-Goto straight string (whose equation of state is $\mu_0 = T$, where $\mu_0$ is the mass per unit length). The equation of state of a wiggly string (averaged over the small-scale structure) is [35,36]

$$\tilde{U}\tilde{T} = \mu_0^2,$$

$$\tilde{U} = \alpha\mu_0, \quad \tilde{T} = \mu_0/\alpha, \tag{2.1}$$

where $\alpha$ is the wiggliness parameter, estimated [23] in the radiation and matter eras to be $\alpha_r \simeq 1.9$ and $\alpha_m \simeq 1.5$, respectively. The expected evolution of the wiggliness parameter is fitted by [23,26]

$$\alpha(\tau) = 1 + \frac{(\alpha_r - 1)a}{\tau\dot{a}}, \tag{2.2}$$

where $a$ is the scale factor.

The parameters of the segments length, velocity, and wiggliness are modeled using the one-scale model [29,30]. Both the evolution of the two competing processes of string stretching (due to cosmic expansion) and the chopping off of loops and their subsequent decay (due to long string reconnection) are described by [37]

$$\frac{dl}{d\tau} = \frac{\dot{a}}{a} l v^2 + \frac{1}{2}\tilde{c} v, \tag{2.3}$$

$$\frac{dv}{d\tau} = (1 - v^2)\left(\frac{\tilde{k}}{l} - 2\frac{\dot{a}}{a} v\right), \tag{2.4}$$

where $l$ is the comoving correlation length, $v$ is the rms string velocity, $\tilde{c}$ is the loop chopping efficiency, and $\tilde{k}$ is the effective curvature of the strings [13]. At every subsequent epoch, a certain fraction of the number of segments decays in a way that preserves scaling.

The Fourier transform of the energy-momentum tensor for an individual string segment $m$ is

$$\Theta_{00}^m = \frac{\mu\alpha}{\sqrt{1 - v^2}} \frac{\sin(k\hat{X}_3' l/2)}{k\hat{X}_3' l/2} \cos(\mathbf{k}\cdot\mathbf{x_0} + k\hat{X}_3 v\tau), \tag{2.5}$$

$$\Theta_{ij}^m = \left[ v^2 \hat{X}_i \hat{X}_j - \frac{(1 - v^2)}{\alpha^2} \hat{X}_i' \hat{X}_j' \right] \Theta_{00}, \tag{2.6}$$

while $\Theta_{0i}^m$ can be found from the relation $\nabla^\mu \Theta_{\mu\nu}^m = 0$. [$X^\mu(\sigma,\tau)$ are the coordinates of the segments $X^0 = \tau$ and $\mathbf{X} = \mathbf{x_0} + \sigma\hat{\mathbf{X}}' + v\tau\hat{\mathbf{X}}$, where $\mathbf{x_0}$ is the random location of the center of mass, $\hat{\mathbf{X}}'$ and $\hat{\mathbf{X}}$ are unit vectors along and perpendicular to the string, which are randomly oriented and also satisfy $\hat{\mathbf{X}}' \cdot \hat{\mathbf{X}} = 0$, and $\sigma$ is the coordinate along the string.]

A consolidation of all string segments that decay at the same epoch into one with the appropriate statistical weight is used, as was suggested in [12], so that the number of segments can be dealt with computationally. The total energy-

momentum tensor of the network is the sum over the contributions of the consolidated string segments [26]

$$\Theta_{\mu\nu}(\mathbf{k},\tau)=\sum_{m=1}^{N_0}\Theta^m_{\mu\nu}(\mathbf{k},\tau)T^{off}(\tau,\tau_m), \tag{2.7}$$

where $N_0$ is the initial number of segments, and $T^{off}$ is a smooth function that turns off the $m$th segment by time $\tau_m$ [12,13]. $\Theta_{\mu\nu}(\mathbf{k},\tau)$ will be incorporated into the sources $S(k,\tau)$ [cf. Eqs. (2.12), (2.14)].

Our main goal is to compute the CMB anisotropy seeded by cosmic strings:

$$\frac{\Delta T}{T}(\hat{\mathbf{n}})\equiv\frac{\Delta T}{T}(\mathbf{x}=0,\hat{\mathbf{n}},\tau_0)=\sum_{l,m}a_{lm}Y_{lm}(\hat{\mathbf{n}}) \tag{2.8}$$

($\mathbf{x}$ is the position of the observer and $\hat{\mathbf{n}}$ is the line of sight direction). The code[1] of [26] (based on CMBFAST[2]), which we modified and used, uses the line of sight integration approach [28] to compute, among other things, the angular power spectrum $C_l$:

$$C_l=\frac{1}{2l+1}\sum_{m=-l}^{l}\langle a^*_{lm}a_{lm}\rangle, \tag{2.9}$$

originating from temperature perturbations seeded by cosmic strings by incorporating the sources into $\Theta_{\mu\nu}$ in the way described below.

The Fourier transform $\Delta(\mathbf{k},\hat{\mathbf{n}},\tau_0)$ of $(\Delta T/T)(\hat{\mathbf{n}})$ depends only on the angle $q$ between the two vectors ($q\equiv\hat{\mathbf{k}}\cdot\hat{\mathbf{n}}$), and can be expanded in multipole moments $\Delta_l(\mathbf{k},\tau_0)$ [38] to

$$\Delta(\mathbf{k},\hat{\mathbf{n}},\tau_0)=\sum_{l=0}^{\infty}(-i)^l(2l+1)\Delta_l(\mathbf{k},\tau_0)P_l(\hat{\mathbf{k}}\cdot\hat{\mathbf{n}}). \tag{2.10}$$

Further, $\Delta_l(\mathbf{k},\tau_0)$ is decomposed into [38]

$$\Delta_l(\mathbf{k},\tau_0)\equiv\xi(\mathbf{k})\Delta_l(k,\tau_0). \tag{2.11}$$

However, according to the line of sight integration approach [28,39],

$$\Delta(k,q,\tau_0)=\int_0^{\tau_0}e^{ikq(\tau-\tau_0)}S(k,\tau)d\tau, \tag{2.12}$$

where the term $S(k,\tau)$ contains the contributions from all the sources, as well as $\Theta_{\mu\nu}$ from the string network [28]. Using the relation

$$e^{ikq(\tau-\tau_0)}=\sum_l(-i)^l(2l+1)j_l[k(\tau_0-\tau)]P_l(q), \tag{2.13}$$

we get [28]

$$\Delta_l(k,\tau_0)=\int_0^{\tau_0}S(k,\tau)j_l[k(\tau_0-\tau)]d\tau. \tag{2.14}$$

In order to get the $a_{lm}$ coefficients needed to construct the maps, we have to assume arbitrary direction for $\hat{\mathbf{k}}$, or equivalently, use the more general relation [43]

$$e^{i\mathbf{k}\cdot\mathbf{r}}=4\pi\sum_{l=0}^{\infty}\sum_{m=-l}^{l}i^l j_l(kr)Y^*_{lm}(\hat{\mathbf{k}})Y_{lm}(\hat{\mathbf{r}}) \tag{2.15}$$

in Eq. (2.10), (2.12). Otherwise, we would be able to compute only the $a_{l0}$ terms (as we shall see next). Then, Eq. (2.14) still holds. The $a_{lm}$'s read [38]

$$\begin{aligned}a_{lm}&=\int d\Omega Y^*_{lm}(\hat{\mathbf{n}})\frac{\Delta T}{T}(\hat{\mathbf{n}})\\&=4\pi(-i)^l\int d^3\mathbf{k}Y^*_{lm}(\hat{\mathbf{k}})\Delta_l(\mathbf{k},\tau_0)\\&=4\pi(-i)^l\int d^3\mathbf{k}Y^*_{lm}(\hat{\mathbf{k}})\xi(\mathbf{k})\Delta_l(k,\tau_0),\end{aligned} \tag{2.16}$$

where $\Delta_l(k,\tau_0)$ is given in Eq. (2.14) [had we not assumed the arbitrariness of $\hat{\mathbf{k}}$, we would only get $a_{lm}=(-i)^l\sqrt{4\pi(2l+1)}\int d^3\mathbf{k}\xi(\mathbf{k})\Delta_l(k,\tau_0)\delta_{m0}=a_{l0}$].

Since the linearized Einstein equations may be decomposed into scalar, vector, and tensor parts $(S,V,T)$ [40], we have three distinct contributions to the sources (e.g., $S$: density perturbations, $V$: cosmic strings, and $T$: gravitational radiation [13,16]). So, $(\Delta,\Delta_l)$ are actually $(\Delta^I,\Delta^I_l)$, where $I\equiv S,V,T$. Then

$$a_{lm}=a^S_{lm}+a^V_{lm}+a^T_{lm}, \tag{2.17}$$

while $C_l=C^S_l+C^V_l+C^T_l$. Following the normalization used in the code, the $a_{lm}$'s are defined as

$$\begin{aligned}a^S_{lm}&=\sqrt{\frac{2}{\pi}}\int d^3\mathbf{k}Y^*_{lm}(\hat{\mathbf{k}})\Delta^S_l(\mathbf{k},\tau_0),\\a^V_{lm}&=\sqrt{\frac{4}{\pi}l(l+1)}\int d^3\mathbf{k}Y^*_{lm}(\hat{\mathbf{k}})\Delta^V_l(\mathbf{k},\tau_0),\\a^T_{lm}&=\sqrt{\frac{4}{\pi}\frac{(l+2)!}{(l-2)!}}\int d^3\mathbf{k}Y^*_{lm}(\hat{\mathbf{k}})\Delta^T_l(\mathbf{k},\tau_0),\end{aligned} \tag{2.18}$$

where $\Delta^I_l(\mathbf{k},\tau_0)\equiv\xi(\mathbf{k})\Delta^I_l(k,\tau_0)$. In order to implement this scheme, we had to extend the code of [26] to provide for the amplitude of the initial perturbations $\xi(\mathbf{k})$, which must be such that [38,39,41]

$$\langle\xi^*(\mathbf{k})\xi(\mathbf{k}')\rangle=P_\xi(k)\delta(\mathbf{k}-\mathbf{k}'), \tag{2.19}$$

where $P_\xi(k)$ is their power spectrum.

[1] http://theory4.phys.cwru.edu/~levon

[2] http://www.sns.ias.edu/~matiasz/CMBFAST/cmbfast.html

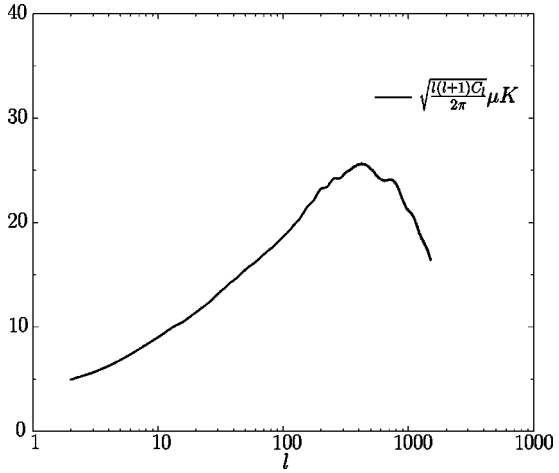


FIG. 1. Angular power spectrum of a $l=1500$ map.

As in [26], we chose the initial power spectrum to be that of white noise, i.e., $P_\xi(k)=$constant. Consequently, $\xi(\mathbf{k})$ was chosen to be proportional to a uniformly random number $\xi_\mathbf{k}\epsilon[-1,1]$. Since: $\langle \xi_\mathbf{k}\xi_{\mathbf{k}'}\rangle=\frac{1}{3}\delta_{\mathbf{k}\mathbf{k}'}$, each $a^I_{lm}$ was multiplied by a factor of $\sqrt{3}$ when the ensemble average $\langle a^{I*}_{lm}a^I_{lm}\rangle$ was taken in order to compute and verify the $C^I_l$'s.[3]

Applying $\int d^3\mathbf{k}'\langle \xi^*(\mathbf{k})\xi(\mathbf{k}')\rangle=P_\xi(k)$ to our discrete case we get $\Sigma_\mathbf{k}\Delta V_\mathbf{k}\langle \xi_\mathbf{k}\xi_{\mathbf{k}'}\rangle=\frac{1}{3}\Sigma_\mathbf{k}\Delta V_\mathbf{k}\delta_{\mathbf{k}\mathbf{k}'}=\frac{1}{3}\Delta V_\mathbf{k}$. This leads to the definition of $\xi(\mathbf{k})$ as

$$\xi(\mathbf{k})\equiv\frac{\xi_\mathbf{k}}{\sqrt{\Delta V_\mathbf{k}}},\quad \xi_\mathbf{k}:\quad \text{random}\ \ \epsilon[-1,1],$$

$$\Delta V_\mathbf{k}\equiv k^2dk\ d\Omega(\hat{\mathbf{k}}). \tag{2.20}$$

Having chosen this particular realization for $\xi(\mathbf{k})$, we can proceed to the construction of the temperature anisotropy maps using Eqs. (2.8), (2.18).

## III. RESULTS

We chose to construct maps with $l=40$, so that the pixel size is comparable to that of the COBE maps, although our method enables us to proceed even up to much higher $l$'s (e.g., $l\simeq 1500$), with greater cost in computational time, though. The angular power spectrum of such a map is depicted in Fig. 1, in agreement with Ref. [26]. A typical example of such a map is depicted in Fig. 2, where a $30°\times 30°$ patch of a standardized temperature anisotropy map is shown.

We have applied statistical tests on the above maps in an attempt to identify possible non-Gaussian features. Such statistical tests [31] have recently been proposed for the detection of the particular type of non-Gaussianity induced by coherent discontinuities (edges) hidden in CMB maps. The main advantage of these statistical tests is that they focus on the large-scale coherent properties of CMB maps, and are therefore effective even in cases of low resolution maps provided that the area covered is large. The statistics calculated for maps of CMB anisotropies seeded by cosmic strings which we have constructed, are the skewness, kurtosis, and the recently devised maximum sample difference (MSD) and sample mean difference (SMD) [31], which are optimized for the detection of coherent discontinuities in 1D and 2D pixel maps. It should be pointed out that the skewness and kurtosis statistics have proven [31] to be notably unsuitable to detect the subtle non-Gaussianity in CMB maps. However, they have been used as a benchmark [31] to test the effectiveness of more complex statistics like the SMD and the MSD, having been specially designed for the detection of specific types of non-Gaussian signatures.

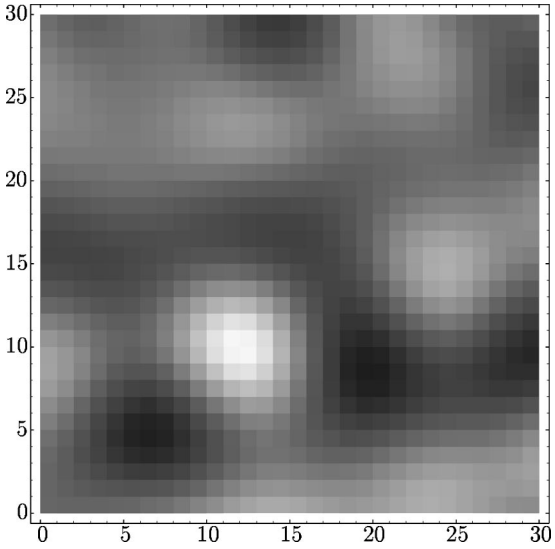


FIG. 2. A $30°\times 30°$ patch of one of the constructed standardized temperature anisotropy maps. (Lighter colors correspond to higher values of $\Delta T/T$).

In addition to the statistics discussed here, there are a number of other more complex statistics [42] (Minkowski functionals as well as bispectrum and higher order cumulant estimates in harmonic space) that may be applied to CMB maps to check for non-Gaussianity or topological signatures of defects. Those statistics which are particularly effective on high resolution CMB maps have been discussed extensively in the literature, and their application on string maps produced by CMBFAST can be an interesting extension of the present work. Here we focus on the MSD and SMD statistics, which are specially designed [9] to detect the specific signature of large scale coherent discontinuities on CMB maps of low resolution.

Assuming a $30°\times 30°$ (in pixels) standardized temperature map $T_{ij}$ $(i,j=1,\ldots 30)$, the skewness $s$ and kurtosis $k$ are defined as

$$s=\langle T^3\rangle\equiv\sum_{i,j}\ T^3_{ij}/(30)^2, \tag{3.1}$$

[3]The $C^I_l$'s are $C^S_l=\frac{2}{\pi}\int k^2dk|\Delta^S_l(k,\tau_0)|^2$, $C^V_l=\frac{4}{\pi}l(l+1)\int k^2dk|\Delta^V_l(k,\tau_0)|^2$, and $C^T_l=(4/\pi)[(l+2)!/(l-2)!]\int k^2dk|\Delta^T_l(k,\tau_0)|^2$.

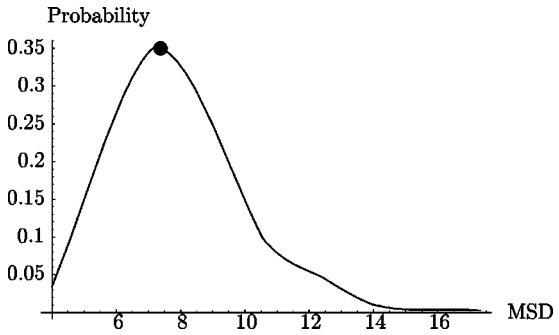


FIG. 3. Probability distribution of the MSD based on 1200 Gaussianized maps. The probability for obtaining the MSD value of the string-induced map (MSD=7.378, represented by the dot) is 0.35.

$$k=\langle T^4\rangle\equiv\sum_{i,j} T_{ij}^4/(30)^2. \tag{3.2}$$

These are conventional statistics, and their values for Gaussian maps with uncorrelated pixels are $s=0,k=3$. To define the statistics MSD and SMD, we consider a partition of the CMB maps in two parts separated by a random curve. In this study we have considered straight lines as well as right angles. Let $\bar{k}$ denote the set of parameters that define the partition line and let $\bar{T}_u$ and $\bar{T}_l$ be the mean temperatures of the two parts of the map (the indices $u$ and $l$ stand for upper and lower parts). The statistical variable $Y_{\bar{k}}$ is defined as

$$Y_{\bar{k}}\equiv|\bar{T}_u-\bar{T}_l|. \tag{3.3}$$

The statistics MSD and SMD are defined as

$$MSD\equiv\frac{1}{N}\sum_{\bar{k}} Y_{\bar{k}}, \tag{3.4}$$

$$SMD\equiv\max(Y_{\bar{k}}), \tag{3.5}$$

where $N$ is the total number of partitions. Both MSD and SMD approach asymptotic values for large $N$. Consider now a Gaussian pattern of temperature fluctuations with a small coherent temperature discontinuity defined by a partition $\bar{k}_0$ superposed on the map, with a coherence scale comparable to the size of the pattern. In [31], it was shown that the presence of such a discontinuity can be detected much more efficiently by the statistics MSD and SMD than by the skewness and kurtosis. A physically motivated mechanism which can lead to the production of a coherent discontinuity on CMB maps is the presence of a long moving cosmic string in our horizon via the aforementioned Gott-Kaiser-Stebbins effect [32,33].

The four statistical tests (MSD, SMD, skewness, and kurtosis) have been performed on patches of the maps (Fig. 2) produced by the simulation in a way similar to the one in [9]: First the values of the four statistical variables were computed for a specific $30°\times30°$ patch obtained using the simulation code; a large number (1200) of Gaussianized maps were constructed from this patch by randomizing the phases in Fourier space and using a Gaussian spectrum with zero mean and variance equal to the measured spectrum of the map; the four statistics were calculated for each of these Gaussianized maps; using these results, the probability distribution for each statistic was constructed; finally, the probability for obtaining the already calculated (in step 1) values of the four statistics was found.

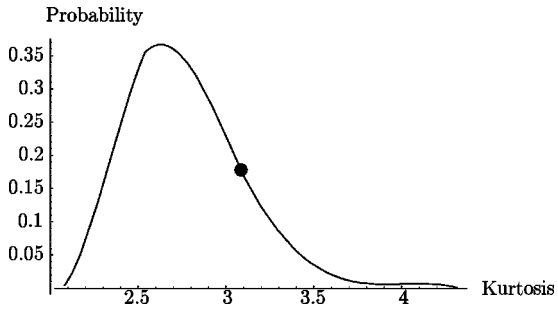


FIG. 4. Probability distribution of the kurtosis based on 1200 Gaussianized maps. The probability for obtaining the kurtosis value of the string-induced map (kurtosis=3.08, represented by the dot) is 0.17.

The results are shown in Figs. 3 and 4. Clearly, the applied statistics cannot reveal non-Gaussianity in a statistically significant amount in the maps produced by the simulation. The values of the statistics considered for the string induced maps (black dots) are within $1\sigma$ in the probability distributions produced by the Gaussianized maps.

We have also extended the above results using right angles as partition lines instead of straight lines. However, the sensitivity of the statistics considered was not increased, rendering results similar to Figs. 3 and 4.

## IV. CONCLUDING REMARKS

String-induced maps on large angular scales are hard to distinguish from maps with Gaussian fluctuations, even using specially designed tests. We have suggested a technique for constructing string-induced temperature anisotropy maps which can be exploited in many ways. The maps constructed via the method described in Sec. II have proven not to be dominated by late long strings. On the contrary, small-scale structure features come into play which, in a way, destructively interfere and ruin the large-scale coherence which the MSD and SMD tests are proposed to optimally detect. Thus, we offered a confirmation to the fact that string-induced temperature anisotropy maps are practically Gaussian on large scales.

## ACKNOWLEDGMENTS

We would like to thank Levon Pogosian and Tanmay Vachaspati for their assistance in acquiring and better understanding the code they developed by modifying CMBFAST.

[1] J. Gott *et al.*, Astrophys. J. **352**, 1 (1990).
[2] R. Moessner, L. Perivolaropoulos, and R. Brandenberger, Astrophys. J. **425**, 365 (1994).
[3] J. Magueijo, Phys. Rev. D **52**, 4361 (1995).
[4] P.G. Ferreira and J. Magueijo, Phys. Rev. D **56**, 4578 (1997).
[5] A. Lewin, A. Albrecht, and J. Magueijo, Mon. Not. R. Astron. Soc. **302**, 131 (1999).
[6] D. Lyth, Phys. Rep. **314**, 1 (1999).
[7] A. Vilenkin and E. Shellard, in *Cosmic Strings and other Topological Defects*, edited by P. Landshoff (Cambridge University Press, Cambridge, England, 1994).
[8] A. Kogut *et al.*, Astrophys. J. Lett. **464**, L29 (1996).
[9] L. Perivolaropoulos and N. Simatos, Mod. Phys. Lett. A **13**, 2945 (1998).
[10] P.G. Ferreira, J. Magueijo, and K. Gorski, Astrophys. J. Lett. **503**, L1 (1998).
[11] U. Pen, U. Seljak, and N. Turok, Phys. Rev. Lett. **79**, 1611 (1997).
[12] A. Albrecht, R. Battye, and J. Robinson, Phys. Rev. Lett. **79**, 4736 (1997).
[13] A. Albrecht, R. Battye, and J. Robinson, Phys. Rev. D **59**, 023508 (1999).
[14] R. Battye, J. Robinson, and A. Albrecht, Phys. Rev. Lett. **80**, 4847 (1998).
[15] C. Contaldi, M. Hindmarsh, and J. Magueijo, Phys. Rev. Lett. **82**, 679 (1999).
[16] N. Turok, U. Pen, and U. Seljak, Phys. Rev. D **58**, 023506 (1998).
[17] U. Pen, U. Seljak, and N. Turok, Phys. Rev. Lett. **79**, 1611 (1997).
[18] U. Seljak, U. Pen, and N. Turok, Phys. Rev. Lett. **79**, 1615 (1997).
[19] A. Riazuelo, N. Deruelle, and P. Peter, Phys. Rev. D **61**, 123504 (2000).
[20] R. Durrer and M. Sakellariadou, Phys. Rev. D **56**, 4480 (1997).
[21] B. Allen *et al.*, Phys. Rev. Lett. **79**, 2624 (1997).
[22] B. Allen *et al.*, Phys. Rev. Lett. **77**, 3061 (1996).
[23] D. Bennett and F. Bouchet, Phys. Rev. D **41**, 2408 (1990).
[24] L. Perivolaropoulos, Phys. Lett. B **298**, 305 (1993).
[25] L. Perivolaropoulos, Astrophys. J. **451**, 429 (1995).
[26] L. Pogosian and T. Vachaspati, Phys. Rev. D **60**, 083504 (1999).
[27] T. Vachaspati and A. Vilenkin, Phys. Rev. Lett. **67**, 1057 (1991).
[28] U. Seljak and M. Zaldarriaga, Astrophys. J. **469**, 437 (1996).
[29] T. Kibble, Nucl. Phys. **B252**, 227 (1985).
[30] T. Kibble, Nucl. Phys. **B261**, 750 (1986).
[31] L. Perivolaropoulos, Phys. Rev. D **58**, 103507 (1998).
[32] J. Gott, Astrophys. J. **288**, 422 (1985).
[33] N. Kaiser and A. Stebbins, Nature (London) **310**, 391 (1984).
[34] D. Bennett, F. Bouchet, and A. Stebbins, Nature (London) **335**, 410 (1988).
[35] B. Carter, Phys. Rev. D **41**, 3869 (1990).
[36] A. Vilenkin, Phys. Rev. D **41**, 3038 (1990).
[37] C. Martins and E. Shellard, Phys. Rev. D **54**, 2535 (1996).
[38] C.P. Ma and E. Bertschinger, Astrophys. J. **455**, 7 (1995).
[39] U. Seljak, Astrophys. J. **482**, 6 (1997).
[40] R. Crittenden and N. Turok, Phys. Rev. Lett. **75**, 2642 (1995).
[41] M. Zaldarriaga and U. Seljak, Phys. Rev. D **55**, 1830 (1997).
[42] J. Magueijo, Phys. Lett. B **342**, 32 (1995); **B352**, 499(E) (1995); P. Ferreira and J. Magueijo, Phys. Rev. D **55**, 3358 (1997); P. Ferreira, J. Magueijo, and J. Silk, *ibid.* **56**, 4592 (1997).
[43] L. D. Landau, in *Quantum Mechanics*, Chap. V, Sec. 34, p. 113.